Michalowski, R. L. (2008). *Géotechnique* **58**, No. 6, 489–501 [**doi:** 10.1680/geot.2007.00055]

Limit analysis with anisotropic fibre-reinforced soil

R. L. MICHALOWSKI*

Fibre reinforcement is a technology to improve the strength of soils used as fill in geotechnical structures. The properties of the fibre-reinforced sand are anisotropic because of the distribution of orientation of the fibres, which is characterised by a preferred bedding plane. The development of an anisotropic yield condition for fibre-reinforced sand is presented. Application of the kinematic approach of limit analysis to anisotropic frictional materials is demonstrated. An interesting implication of anisotropy is a lack of uniqueness in the internal friction angle along a shear surface with given orientation. The anisotropic internal friction angle was found to be a function of the major principal strain rate direction, and not just a function of the orientation of the shear surface. While the inclination of principal strain rate directions can be inferred from the kinematics of the mechanism for a given boundary value problem, the internal friction angle cannot be determined *a priori* as a unique function of orientation in space. Two examples are presented to illustrate the use of the kinematic approach for anisotropic frictional materials: retaining wall loading, and the bearing capacity of a footing.

KEYWORDS: anisotropy

Le renforcement aux fibres est une technique utilisée pour renforcer la résistance des sols employés pour le remblayage de structures géotechniques. Les propriétés du sable renforcé aux fibres sont anisotropes, en raison de la distribution de l'orientation des fibres, caractérisée par un plan de stratification préféré. Le développement d'une limite élastique anisotrope pour le sable renforcé aux fibres est présenté. On démontre l'application d'une méthode cinématique de l'analyse des limites pour des matières à friction anisotropes. Une implication intéressante de l'anisotropie est l'absence d'unicité dans l'angle de friction interne, le long d'une surface de cisaillement présentant une orientation donnée. On a relevé que l'angle de friction anisotrope interne est tributaire de la direction principale de la vitesse de déformation, et non pas simplement de l'orientation de la surface de cisaillement. Tandis que l'inclinaison des directions principales de la vitesse de déformation peut être subie par la cinématique du mécanisme, pour un problème donné de valeur limite, l'angle de friction interne ne peut, à priori, être déterminé comme une fonction unique de l'orientation dans l'espace. Deux exemples sont présentés pour illustrer l'emploi de principes de cinématique pour des matières à friction anisotropes : la charge de murs de soutènement et la force portante d'une semelle.

INTRODUCTION

The reinforcement of soils with short fibres is a technology for soil improvement that has not been fully utilised in engineering practice. The interest in fibre reinforcement of soils began in the 1970s with an attempt to estimate the influence of plant and tree roots on the stability of earth slopes (Waldron, 1977). Subsequent models were based on analysis of a single fibre intersecting a band of soil with localised shear strain (Gray & Ohashi, 1983; Maher & Gray, 1990; Zornberg, 2002). While these efforts revealed the complexity of the soil–fibre interaction, they did not come to fruition in the form of the yield condition in terms of the components of the stress tensor. Consequently, these early models did not find implementation in numerical tools, such as the finite element method.

Efficient and quite accurate estimates of the contribution of fibres to the soil strength have been made for isotropic reinforced soils where fibres were assumed to be distributed evenly in all directions (Michalowski & Zhao, 1996; Michalowski & Čermák, 2003). However, because of the technology of deposition of fibre-reinforced soils (in situ mixing, rolling, compacting), the fibre orientation clearly has a preferred bedding plane, giving rise to anisotropy of the mechanical properties of the mixture.

A composite similar to fibre-reinforced soils was developed in the 1980s, with a continuous filament used in place of short fibres (e.g. Leflaive & Liausu, 1986; di Prisco & Nova, 1993). Although the interaction mechanism of soil and continuous filament differs from that in short fibre mixtures, the description of the anisotropic distribution of orientation used for the filament (Michalowski, 1997a) was later adopted for fibre reinforcement (Michalowski & Čermák, 2002). This paper builds on these earlier results.

The effort here is concentrated on the development of an anisotropic yield condition for fibre-reinforced sand, and on the application of the kinematic approach of limit analysis to solving problems with anisotropic materials.

A yield condition for sand with an ellipsoidal distribution of the fibre orientation is presented in the next section. The plastic state, kinematic discontinuities, and internal friction angle in anisotropic composites are then discussed. Finally, a construction of kinematically admissible mechanisms is shown, and numerical examples are presented.

YIELDING OF ANISOTROPIC FIBRE-REINFORCED SAND

The soil under consideration is granular (sand), and the fibres are at least one order of magnitude longer than the size of an average grain. The thickness of the fibres is at least of the same order of magnitude as the size of an average grain, so that the assumption of the frictional soil–fibre interaction is reasonable.

Stress in fibres and work dissipation during slip

The primary mechanism of fibre–sand interaction is considered here to be frictional, with ϕ_w being the interface friction angle (constant). The earlier experimental results

Manuscript received 7 April 2007; revised manuscript accepted 23 January 2008.
Discussion on this paper closes on 2 February 2009, for further details see p. ii.
* Department of Civil and Environmental Engineering, The University of Michigan, Ann Arbor, USA.

confirm such an assumption to be reasonable (Michalowski & Zhao, 1996; Michalowski & Čermák, 2003). It is also assumed that, at the instant of composite failure, the fibres behave as rigid–perfectly plastic inclusions. This does not imply that the fibres do not deform elastically prior to the composite's reaching the limit state. However, at the limit state, the stiffness of the composite drops down to zero, and the incipient failure mechanism is not associated with an increase in the fibre elastic energy (a purely dissipative process).

The fibres will slip during plastic deformation of the matrix material, inducing axial stress σ_f in the fibres. Equilibrium of an infinitesimal element in Fig. 1(b) leads to

$$\frac{d\sigma_f}{dx} = -\frac{2\tau}{r} \tag{1}$$

and, for the boundary condition $\sigma_f = 0$ at $x = l/2$, the solution to this differential equation ($l/2 \geqslant x \geqslant 0$) becomes (tension positive)

$$\sigma_f = \frac{2\tau}{r}\left(\frac{l}{2} - x\right) \tag{2}$$

with r being the radius of the cylindrical fibre and l being its length. This distribution is illustrated in Fig. 2(b), and the shear stress distribution on the fibre surface is shown in Fig. 2(a). However, if the confining stress is large enough (leading to large shear stress τ on the fibre surface), the axial stress σ_f in equation (2) may reach the yield point σ_0 of the fibre material at some $0 < x < l/2$, in which case the fibre will plastically deform (stretch) in its middle portion, consistently with the deformation of the matrix. Hence no slip will occur over the mid section of the fibre, as indicated in Fig. 2(c), and the axial fibre stress will remain constant in that portion (Fig. 2(d)). Previous experimental tests (Maher & Gray, 1990; Michalowski & Zhao, 1996) have indicated that, under the stress conditions commonly found in geotechnical engineering, the yield point of the fibre material is typically not reached: therefore we shall consider further only the case in Figs 2(a) and 2(b). This issue will be discussed further in the section 'The yield surface'. Consideration of the combined slip and yielding of the fibre material illustrated in Figs 2(c) and 2(d) can be found in Michalowski & Zhao (1996).

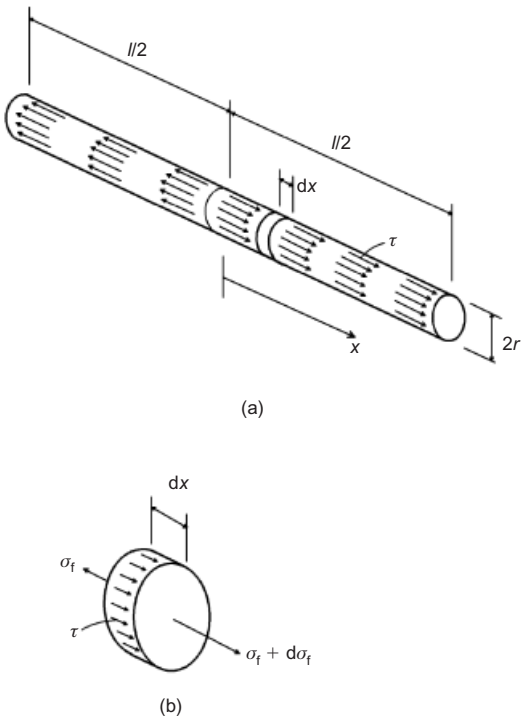

Fig. 1. (a) Shear stress on the fibre surface; (b) an infinitesimal element

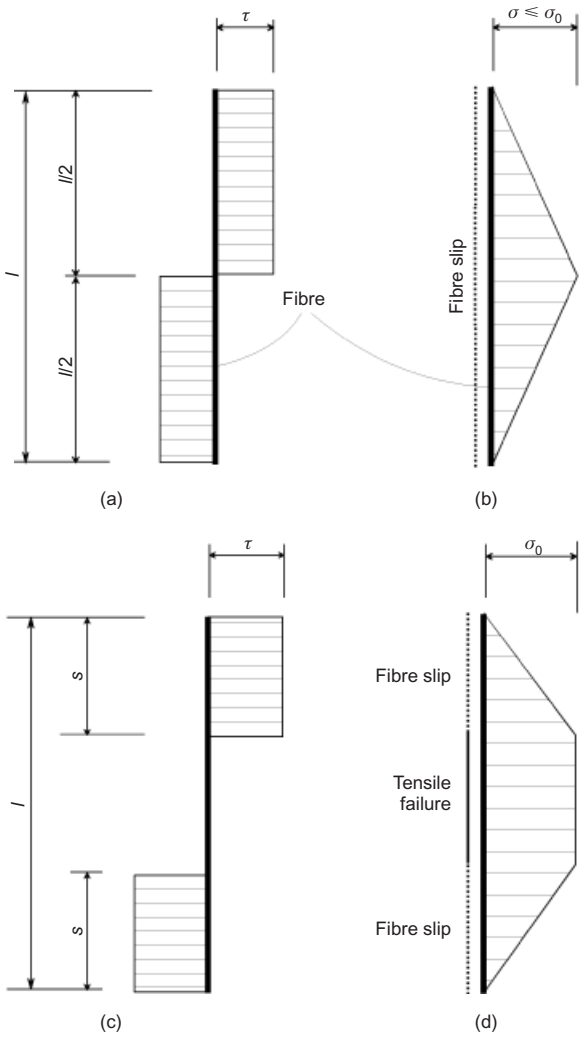

Fig. 2. (a) Idealised shear stress distribution on the surface of a fibre slipping in a deforming matrix; (b) axial stress in a fibre during pure slip; (c) idealised shear stress on a fibre failing in tension; (d) axial stress

Assume that the strain rate in the matrix material (sand) in the direction of a single fibre inclined at θ to plane xOz is $\dot{\varepsilon}_\theta$. The soil mechanics compression positive convention is used for the sand and the composite. The work during fibre slip in the matrix will contribute to the composite strength increase; however, fibres in compression will kink and will not contribute to the strength increase. Therefore, for the purpose of calculating the contribution of a fibre to the composite strength, we define deformation rate $\langle\dot{\varepsilon}_\theta\rangle$ along a single fibre of inclination θ as

$$\langle\dot{\varepsilon}_\theta\rangle = \begin{cases} |\dot{\varepsilon}_\theta| & \text{if } \dot{\varepsilon}_\theta < 0 \quad \text{extension} \\ 0 & \text{if } \dot{\varepsilon}_\theta \geqslant 0 \quad \text{compression} \end{cases} \tag{3}$$

The distribution of slip rate along a single rigid fibre embedded in the matrix subjected to uniform extension $\langle\dot{\varepsilon}_\theta\rangle$ is indicated in Fig. 3, with the maximum at both ends equal to $\langle\dot{\varepsilon}_\theta\rangle l/2$, and with the mid-point of the fibre moving with the same velocity as the matrix (zero slip). Such slip distribution guarantees the minimum internal work rate dur-

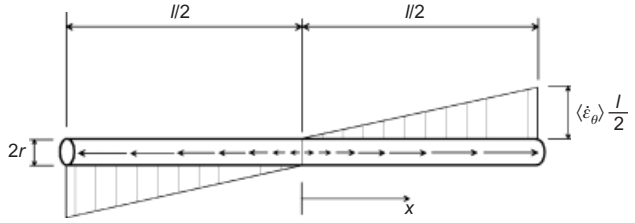

Fig. 3. Distribution of slip rate along a single fibre embedded in a deforming matrix

ing the slip. The fibres are cylindrical in shape, and the normal stress on the fibre surface is considered to be approximately uniform, $\bar{\sigma}_n$. No adhesion of fibres to the matrix is considered, and the slip on the fibre/matrix interface is assumed to be governed by the non-associative rule (no dilation). The work rate during fibre slip integrated over the entire fibre surface then becomes

$$d_f = \frac{1}{2}\pi r l^2 \langle \dot{\varepsilon}_\theta \rangle \bar{\sigma}_n \tan \phi_w \tag{4}$$

where ϕ_w is the fibre/matrix interface friction angle. The plastic work during the deformation of a composite element will include dissipation along all fibres, which are inclined at different angles θ and subjected to different $\langle \dot{\varepsilon}_\theta \rangle$. An orientation of fibres producing anisotropic strength of the composite is considered in the next section.

Characterisation of fibre orientation

Because of rolling and compacting of fibre-reinforced soils during their deposition, the fibres are expected to assume an orientation with the preferred plane being typically horizontal. The average fibre concentration $\bar{\rho}$ is defined as

$$\bar{\rho} = \frac{V_r}{V} \tag{5}$$

where V_r is the volume of the fibres in an element of volume V. The fibres are cylindrical in shape, and are characterised by their aspect ratio η, given by

$$\eta = \frac{l}{2r} \tag{6}$$

where l and r are the fibre length and radius respectively.

A hypothetical distribution of fibres used in earlier investigations (Michalowski, 1997a, Michalowski & Čermák, 2002) was assumed to be axisymmetric, and described in the form

$$\rho(\theta) = \bar{\rho}(A + B|\cos^n \theta|) \tag{7}$$

where $\bar{\rho}$ is the average concentration of the fibres; A, B and n are constant coefficients; and θ is an angle of fibre inclination to the preferred bedding plane. Because the average concentration $\bar{\rho}$ must be equal to

$$\bar{\rho} = \frac{1}{V}\int_V \rho(\theta) \mathrm{d}V \tag{8}$$

only two of the three coefficients in equation (7) are independent (V is the volume of the physical composite element): hence

$$B = \frac{1 - A}{\int_0^{\pi/2} \cos^{n+1}\theta \mathrm{d}\theta} \tag{9}$$

A special case of this function with $n = 2$ and $A = 0$ (i.e. no fibres (filament) in the vertical direction),

$$\rho(\theta) = \frac{3}{2}\bar{\rho}\cos^2\theta \tag{10}$$

was used earlier in the description of inclination of continuous filament reinforcement (Michalowski, 1997a). This function is shown as one of three distributions in Fig. 4(a). The form of the fibre distribution function in equation (7) (and its special case in equation (10)) originated from intuitive considerations that fibre-reinforced soil subjected to compaction, for instance by rolling, will have no vertical fibres, with the horizontal being the preferred bedding plane. This seems to be a reasonable assumption: recent experiments indicated that fibres in specimens prepared by the moist tamping method contained 97% of fibres with an orientation that was within $\pi/4$ of the horizontal plane (Diambra *et al.*, 2007).

Even in the special case of isotropic distribution of the fibres, the ratio of the amount of fibres close to the vertical

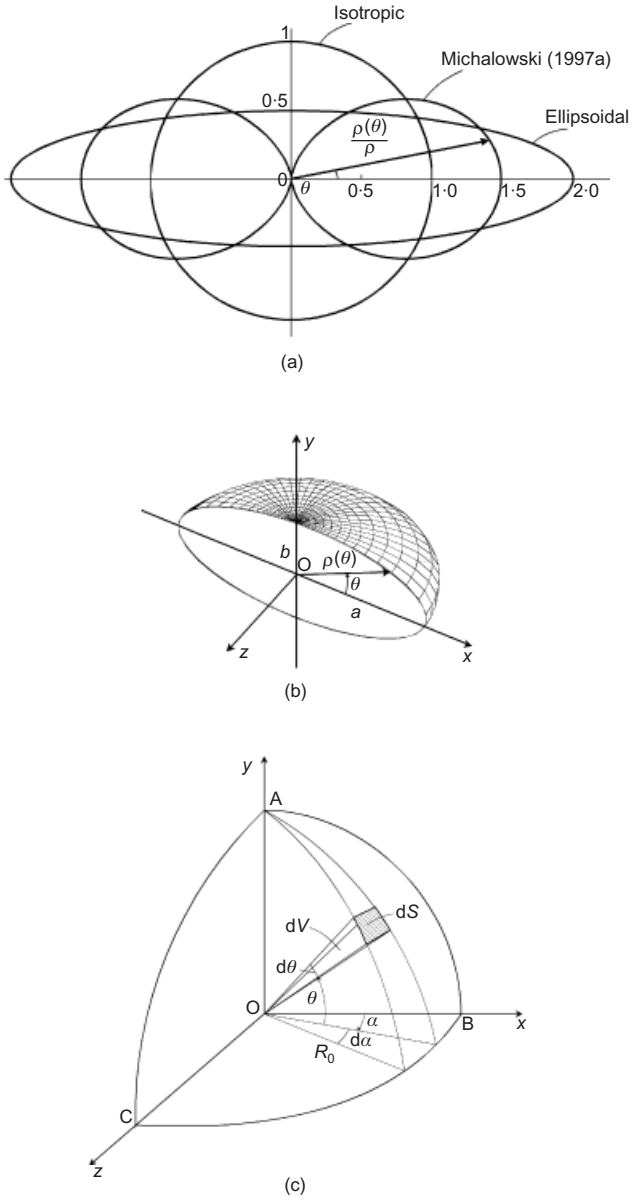

Fig. 4. (a) Hypothetical distributions of fibre orientation; (b) ellipsoidal distribution with preferred bedding plane xOz; (c) spherical octant element

direction is small compared with fibres that are close to the horizontal plane. In a trivial proof one can show that the ratio of the volume of fibres within a range of angle θ to the vertical, to the volume of fibres within the range of θ from the horizontal plane is equal to $\tan(\theta/2)$. For instance, the ratio of respective volumes within 10° of the vertical direction and within 10° of the horizontal plane is only 0·088.

The distributions of fibres in engineering applications are, no doubt, anisotropic; however, there has been little effort, so far, to measure and describe this distribution experimentally. The recent paper by Diambra *et al.* (2007) is the first systematic effort toward this goal. Diambra *et al.* (2007) indicated that specimens prepared by moist tamping (which might be representative of field compaction by dynamic plate compactors) can be well described by a function of the type in equation (7). The distribution of orientation of fibres in lightly compacted composites (e.g. in applications such as veneer layers on slopes) might be represented alternatively by functions other than that in equation (7), for instance, an ellipsoid. Such a distribution will be explored in this paper. Nevertheless, the framework presented for 'averaging' stresses in the composite at failure can accommodate any distribution represented by an analytical function.

The orientation of fibres considered here is graphically presented in Fig. 4(b). This ellipsoidal distribution can be represented as

$$\rho(\theta) = \frac{ab}{\sqrt{a^2 \sin^2\theta + b^2 \cos^2\theta}} \tag{11}$$

where a and b are the half-axes of the elliptical cross-section, and angle θ is the inclination angle to the preferred bedding plane xOz. Half-axes a and b are not convenient measures of orientation distribution, and the aspect ratio of the distribution is introduced as

$$\zeta = \frac{b}{a} \tag{12}$$

Half-axes a and b now can be expressed as functions of $\bar{\rho}$ and ζ, using the average concentration expressed in equation (8). Assume a spherical composite element of radius R_0 with the differential volume element $\mathrm{d}V = (R_0^3 \cos\theta \, \mathrm{d}\alpha \, \mathrm{d}\theta)/3$ (Fig. 4(c)). Because the fibre distribution is axisymmetric with respect to y (independent of α), the average fibre content in equation (8) can be transformed into

$$\bar{\rho} = \frac{1}{2}\int_{-\frac{\pi}{2}}^{\frac{\pi}{2}} \rho(\theta)\cos\theta \mathrm{d}\theta \tag{13}$$

and, after replacing $\rho(\theta)$ with the distribution in (11),

$$\bar{\rho} = \frac{a\zeta}{2}\int_{-\frac{\pi}{2}}^{\frac{\pi}{2}} \frac{1}{\sqrt{\zeta^2 + \tan^2\theta}} \, \mathrm{d}\theta = \frac{a\zeta}{2} I_1(\zeta) \tag{14}$$

Hence

$$a = \frac{2\bar{\rho}}{\zeta I_1}, \qquad b = \frac{2\bar{\rho}}{I_1} \tag{15}$$

Integral I_1 does not have a convenient closed form, and its numerical values are given in Fig. 5 for a practical range of ratio ζ. The composite becomes isotropic when $\zeta = 1$ (for which $I_1 = 2$), and the distribution has a preferred direction of orientation when $\zeta > 1$. For the latter case integral I_1 can be evaluated in a closed form:

$$I_1 = \frac{2\arctan\sqrt{\zeta^2 - 1}}{\sqrt{\zeta^2 - 1}}, \qquad \zeta > 1 \tag{16}$$

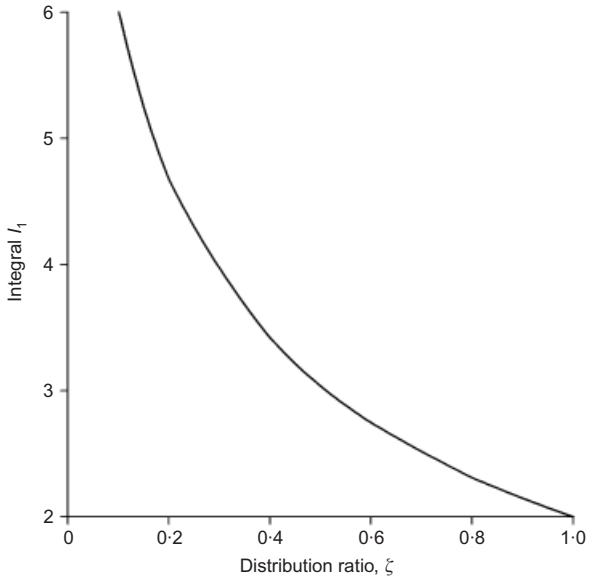

Fig. 5. Integral I_1 as a function of the distribution ratio ζ

The ellipsoidal distribution function is explored here as an alternative to earlier proposed functions, with the goal of developing a yield condition for the fibre-reinforced sand, suitable for use in limit analysis.

Development of the yield condition

The yield condition will be derived using the requirement that in an incipient plastic deformation process of a representative element (Fig. 6), the rate of work of the external load is equal to the rate of plastic work, the latter being dissipated during the fibres slipping in the matrix material

$$\bar{\sigma}_{ij}\dot{\bar{\varepsilon}}_{ij} = \frac{1}{V}\int_V D(\dot{\varepsilon}_{ij})\mathrm{d}V \tag{17}$$

where $\bar{\sigma}_{ij}$ and $\dot{\bar{\varepsilon}}_{ij}$ are the macroscopic (or average) stress state and strain rate tensors in the composite, and $D(\dot{\varepsilon}_{ij})$ is the rate of work dissipation in the composite constituents

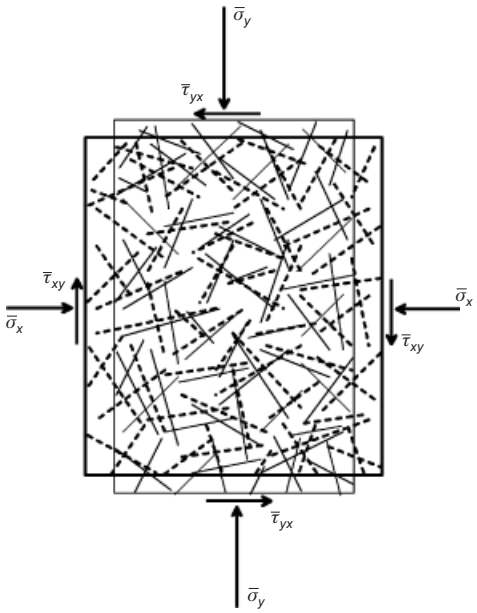

Fig. 6 Uniform deformation of an anisotropic composite element

and on the interfaces between the constituents. There are two plastic flow rules used in this averaging technique: the first governs deformation of the matrix, and the second describes the slip of fibres in the matrix. The deformation of the matrix alone is governed by normality, but the fibre slip is taken as non-associative (no dilatancy). The non-associative slip rule leads to the dependence of dissipation on the stress level.

The strength of the sand (matrix of the composite) is governed by the Mohr–Coulomb yield condition with internal friction angle ϕ. The first important assumption, consistent with the assumed deformation rules, is that the deformation of the composite element in Fig. 6 is uniform, and governed by the flow rule in which the yield condition for the matrix alone plays the role of the plastic potential. Such an assumption, of course, results in non-associative deformation for the composite. For the plane strain condition, the ratio of the principal strain rates becomes

$$\frac{\dot{\bar{\varepsilon}}_3}{\dot{\bar{\varepsilon}}_1} = -\tan^2\left(\frac{\pi}{4}+\frac{\phi}{2}\right) = -K_{\mathrm{p}} \tag{18}$$

The second major assumption is that the normal stress on a single fibre can be approximated by the average in-plane stress in the composite, independent of the fibre orientation. This approximation is used to derive the general expression for the dissipation rate (see the Appendix). The homogenisation scheme in equation (17) was used earlier, and it was found to yield quite a reasonable yield condition in terms of the macroscopic stress for isotropic fibre-reinforced soil (Michalowski & Zhao, 1996). Here, however, the distribution of the fibre orientation causes the composite to have anisotropic strength properties.

An alternative way to average stresses in equation (17) is to assume associative fibre slip. In the absence of fibre–matrix adhesion, the slip normality would produce zero dissipation, but it would contribute to dilatancy in addition to the volume increase produced in the sand alone. In this case the fibre and interface properties would enter the left-hand side of equation (17) through an altered average composite strain rate. A difficulty with such an approach is in the transfer of the dilatancy caused 'locally' by the slip of fibres to the description of the average strain rate components for the entire composite element. Such transfer of strain rate from 'micro' to macro description would require an assumption that would be no less 'decisive' than the one regarding average stress on the fibres.

The consequence of anisotropy is a lack of coaxiality of the stress and strain rate tensors, and the scheme for calculating the macroscopic stresses at failure becomes more elaborate (Michalowski, 1997a; Michalowski & Čermák, 2002). The deformation in the averaging method (Fig. 6) is assumed such that the vertical and horizontal are the principal strain rate directions, but the principal macroscopic stress directions are now inclined at some angle of 'non-coaxiality' m to the directions of the principal strain rates (Fig. 7). This inclination is affected by the distribution of orientation of fibres.

In order to utilise equation (17), the rate of work dissipation on the right-hand side needs to be evaluated. The work rate for a single fibre, d_{f}, was estimated in equation (4), and the dissipation D_{f} integrated over all fibres, excluding those under compression, is presented in the Appendix.

The yield condition is sought in the form

$$f(\bar{\sigma}_x, \bar{\sigma}_y, \bar{\tau}_{xy}) = R - F(p, \psi) = 0 \tag{19}$$

where R is the maximum shear stress (or the radius of the limit Mohr circle)

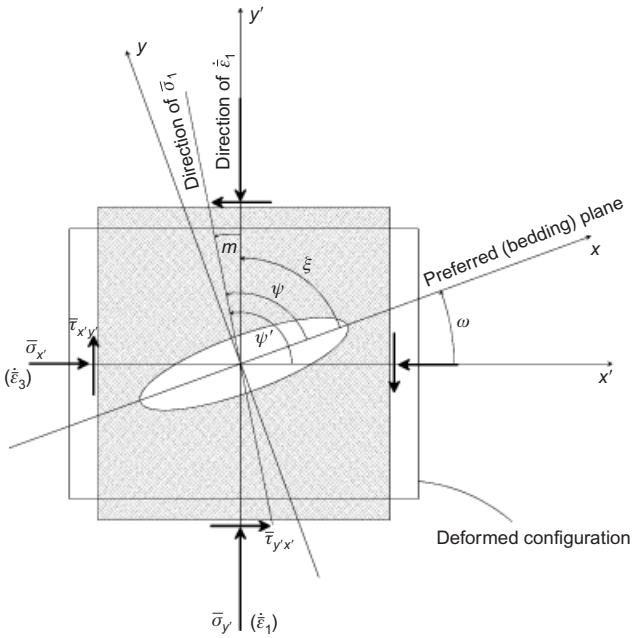

Fig. 7. Deformation of an anisotropic fibre-reinforced soil element

$$R = \frac{1}{2}\left[(\bar{\sigma}_x - \bar{\sigma}_y)^2 + 4\bar{\tau}_{xy}^2\right]^{\frac{1}{2}} \tag{20}$$

p is the in-plane mean macroscopic stress

$$p = \frac{1}{2}(\bar{\sigma}_x + \bar{\sigma}_y) \tag{21}$$

and ψ is the angle of inclination of the major principal stress to axis x

$$\tan 2\psi = \frac{\bar{\tau}_{xy}}{\bar{q}} = \frac{2\bar{\tau}_{xy}}{\bar{\sigma}_x - \bar{\sigma}_y} \tag{22}$$

In the description of anisotropic materials, axis x with respect to which angle ψ is measured must be uniquely related to the physical space, that is, to the pattern of anisotropy (for instance, to the trace of the fibres' preferred bedding plane). When function F in equation (19) is independent of ψ, the yield condition becomes isotropic. In an incipient deformation process of the element in Fig. 7, the principal directions of the strain rate tensor coincide with the horizontal and vertical axes x' and y'. However, the composite is anisotropic: thus the principal directions of the macroscopic stress tensor that causes this deformation will, in general, deviate from the principal directions of the strain rate. Equation (17) is now rewritten in the form

$$\bar{\sigma}_{x'}\dot{\bar{\varepsilon}}_{x'} + \bar{\sigma}_{y'}\dot{\bar{\varepsilon}}_{y'} + 2\bar{\tau}_{x'y'}\dot{\bar{\varepsilon}}_{x'y'} = D_{\mathrm{f}} \tag{23}$$

where the last term on the left-hand side is zero because there is no distortion in coordinate system x', y'. Now introduce q'

$$q' = \frac{\bar{\sigma}_{x'} - \bar{\sigma}_{y'}}{2} = R\cos 2\psi' \tag{24}$$

where ψ' is the angle of inclination of the major principal stress to axis x'. Recalling the definition of p in equation (21), one obtains $\bar{\sigma}_{x'} = p + q'$ and $\bar{\sigma}_{y'} = p - q'$, and, noting that $\dot{\bar{\varepsilon}}_{x'} = \dot{\bar{\varepsilon}}_3$, $\dot{\bar{\varepsilon}}_{y'} = \dot{\bar{\varepsilon}}_1$, and $\dot{\bar{\varepsilon}}_{x'y'} = 0$, the expression in equation (23) takes the form ($p = p'$ since it is invariant)

$$q'\left(\dot{\bar{\varepsilon}}_3 - \dot{\bar{\varepsilon}}_1\right) + p\left(\dot{\bar{\varepsilon}}_3 + \dot{\bar{\varepsilon}}_1\right) = D_{\mathrm{f}} \tag{25}$$

Coordinate system x', y' is the principal strain rate system, whereas the failure criterion must be derived in reference to the physical space (i.e. anisotropy pattern). The plane of preferred fibre orientation (bedding plane) considered here is perpendicular to the plane of deformation, and its trace in Fig. 7 is marked by axis x.

Considering that the Mohr–Coulomb failure criterion used to describe the granular matrix is independent of the intermediate principal stress, the failure criterion for the composite is also expected to be independent of $\bar{\sigma}_z$. The failure criterion then will depend on three independent stress components $\bar{\sigma}_x$, $\bar{\sigma}_y$, and $\bar{\tau}_{xy}$, with direction x uniquely related to the anisotropy pattern (bedding plane).

The yield condition is sought in the form of equation (19), and the general equation (17) will be used to calculate the macroscopic stress at failure, $\bar{\sigma}_{ij}$. However, calculating the work of $\bar{\sigma}_{ij}$ is not straightforward, because the angle by which the principal axes of the stress state deviate from the principal axes of the strain rate tensor is not known *a priori*. It was found convenient to formulate the problem in the following manner: given the major principal stress direction at failure ψ, what would the preferred plane of fibre orientation ω need to be in order for the principal directions of the strain rate to be x' and y' ? Angle ω is defined here as an angle between axis x' and axis x (axis x coincides with the physical plane of preferred fibre orientation). Because R is an in-plane invariant, one can write

$$R = \frac{q}{\cos 2\psi} = \frac{q'}{\cos 2\psi'} = \frac{q'}{\cos 2(\psi + \omega)} \tag{26}$$

and, evaluating q' from equation (25), and eliminating $\dot{\bar{\varepsilon}}_3$ using equation (18), the following expression results

$$R = -\left(\frac{D_f}{\dot{\bar{\varepsilon}}_1}\frac{1 - \sin\phi}{2} + p\sin\phi\right)\frac{1}{\cos 2(\psi + \omega)} \tag{27}$$

where D_f is expressed in equation (52). Resulting R is always positive, as the cosine in equation (27) is negative. Because the method based on equation (17) is essentially the kinematic approach of limit analysis, the minimum of R is sought from equation (27), with angle ω being variable.

Isotropic fibre-reinforced soil is a special case of the model presented here, where $a = b = \bar{\rho}$ in equation (11), in which case function F in equation (19) becomes independent of ψ. It is possible, for this isotropic case, to obtain a relatively simple closed-form solution to R

$$R = p\left(\sin\phi + \frac{1}{3}N\bar{\rho}\eta\tan\phi_w\right) \tag{28}$$

where

$$N = \frac{1}{\pi}\cos\phi + \left(\frac{1}{2} + \frac{\phi}{\pi}\right)\sin\phi \tag{29}$$

The reader will find derivation of this expression in Michalowski & Zhao (1996).

THE YIELD SURFACE

The yield function in equation (19) is schematically presented in space $\bar{\tau}_{xy}$, q, p in Fig. 8. Both R and ψ have a clear interpretation in the cross-section p = constant in Fig. 8(b). The composite has no shear strength ($R = 0$) when the confining stress is zero, which is consistent with the frictional nature of the matrix and the fibre/matrix interface, and it is confirmed by experiments (e.g. Maher & Gray, 1990). The failure of fibres was assumed to occur in the slip mode, and the surface does not exhibit any discontinuity in the derivative with respect to the mean stress. Such a discontinuity could be caused by the transition of the fibre failure mode from the slip to slip-and-yielding. Some experimental results in the literature exhibit non-linear failure envelopes, typically interpreted as 'bilinear,' with the conjecture that the abrupt change in the derivative is associated with the fibres yielding. This conjecture was put to the test by Maher & Gray (1990), who tested sand reinforced with glass fibres, 0·3 mm in diameter, with tensile strength of $1{\cdot}25 \times 10^6$ kPa and stiffness $7{\cdot}0 \times 10^7$ kPa. These fibres were intact after all tests, yet the failure envelopes had very clear non-linear (or bilinear) characteristics. Maher (1988) remarks that 'fiber rupture or breakage was not observed at any time ... despite the fact that the failure envelopes were displaced upwards, but nevertheless still parallel to those of unreinforced sand at stresses exceeding the critical confining stress.' Clearly, the critical confining stress characterised by the discontinuity in the derivative of the failure envelope was not indicative of the fibre failure mode switching from slip to slip-and-rupture. Maher (1988) indicated that earlier tests by others also revealed no rupture of fibres, and pointed to a possible explanation offered by Hausmann (1976), who noted that the frictional resistance of fibres may drop down

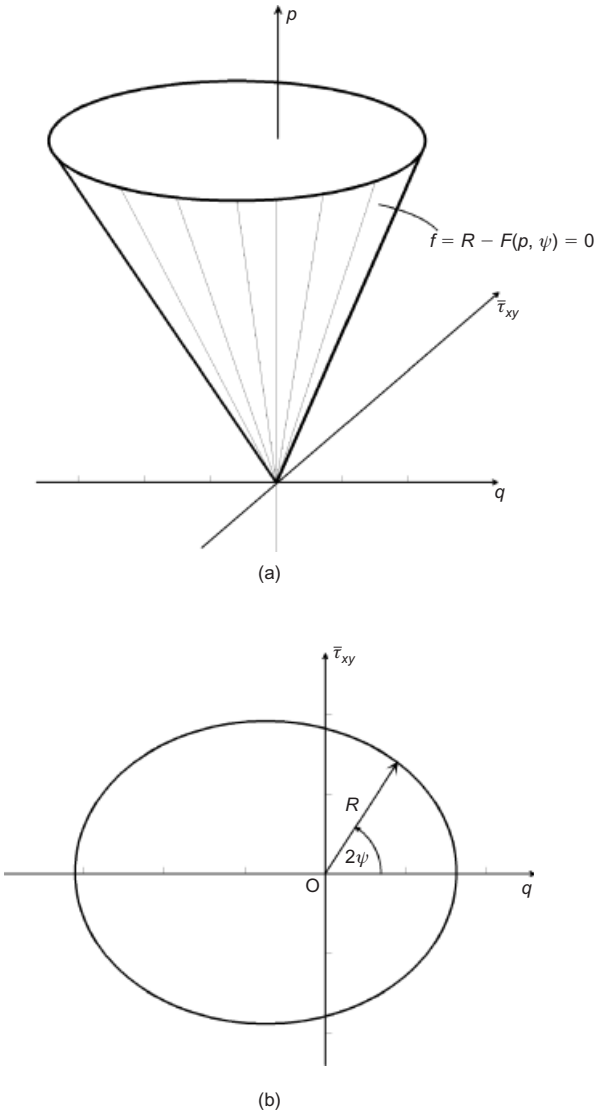

Fig. 8. (a) Hypothetical yield surface for anisotropic soil in space p, q, $\bar{\tau}_{xy}$; (b) cross-section p = constant

at higher stresses as the diameter of highly strained fibres decreases.

A plausible explanation of the non-linearity in the failure envelopes may be found in sand arching around fibres, which prevents transfer of stress to fibres at large loads (larger than 'critical'). To some extent, such an explanation is substantiated by differences in the shape of the failure envelopes for angular and rounded sands, since arching is affected by angularity of grains and uniformity of grain size. Such differences are clearly found in test results by Maher & Gray (1990) for angular and well-graded mortar sand, and rounded, uniform Muskegon dune sand, both reinforced with glass fibres.

Few reports in the literature have quantitative information on the actual rupture (breakage) of fibres. Consoli *et al.* (2005) demonstrated that very thin polypropylene fibres (0·023 mm) can rupture even under isotropic compression. The mechanism of fibre–grains interaction with such thin fibres (aspect ratio of about 10^3) is more typical of continuous filament (e.g. Michalowski, 1997a), and it is not considered here. The yield surface in this paper is developed for fibres that fail in the slip mode, with a thickness of at least the same order of magnitude as the size of an average grain.

The development of the yield condition is numerical in nature, and it requires that points on the yield surface be identified, each through minimising R in equation (27) for given p and ψ, with ω being variable. A single point on the yield surface is described by R and 2ψ (for constant p). Example calculation results are illustrated in Fig. 9(a) for two distribution ratios, $\zeta = 0{\cdot}2$ and $\zeta = 0{\cdot}5$, in addition to the isotropic case, $\zeta = 1$. The following parameters were taken in calculations: $\phi = 36°$, $\phi_w = 24°$, $\eta = 100$, $\bar{\rho} = 0{\cdot}02$ (2%), and $p = 100$ kPa.

It appears from numerical calculations that the cross-section of the yield surface remains approximately circular with the drop in distribution ratio ζ, but that the radius increases slightly, and the origin translates in the direction of negative q. This is illustrated in Fig. 9(b), with R_0 being the radius of the cross-section and Q being the offset of the cross-section centre O′. Both R_0 and Q are dependent on the sand and fibre properties (ϕ, $\bar{\rho}$, η, ϕ_w, and the distribution ratio ζ). The analysis revealed that the number of independent parameters can be reduced to the following three: ϕ, product $\bar{\rho}\eta\tan\phi_w$, and ζ. Variation of R_0 and Q for the composite with matrix internal friction angle $\phi = 30°$ is presented in Fig. 10. Numerical values of R_0/p and Q/p for some ranges of sand and fibre properties are given in Table 1.

One might intuitively expect that, with the content of fibres being constant ($\bar{\rho}$) and only the distribution ratio changing, the size of the yield condition trace on plane $\bar{\tau}_{xy}$, q would remain constant, and the anisotropy would enter through translation Q of the surface, similar to a purely kinematic hardening process. However, with the change in distribution of fibre orientation (ζ), the portion of fibres subjected to tension (contributing to the strength) varies, giving rise to an increase in the size of the yield surface in addition to its translation.

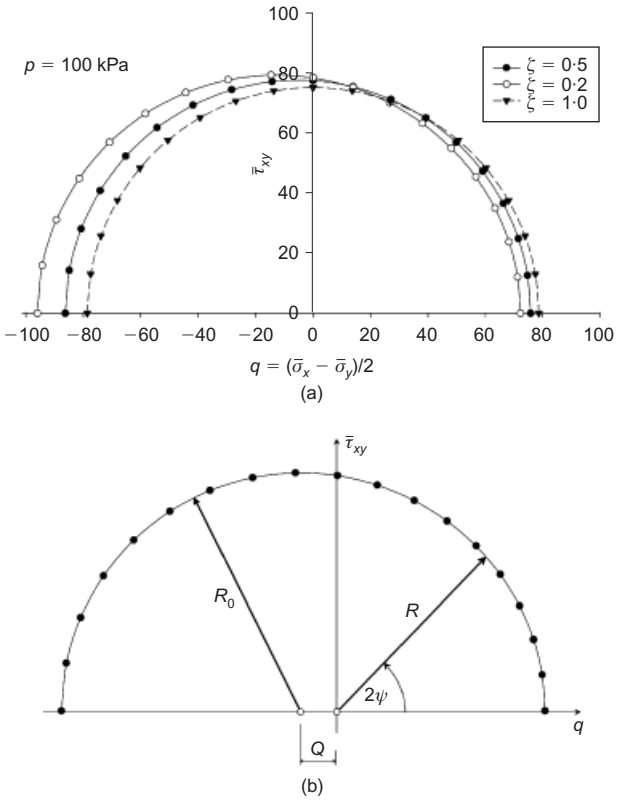

Fig. 9. (a) Calculated points on the yield surface in plane q, $\bar{\tau}_{xy}$ (p = const.); (b) definition of R_0 and Q

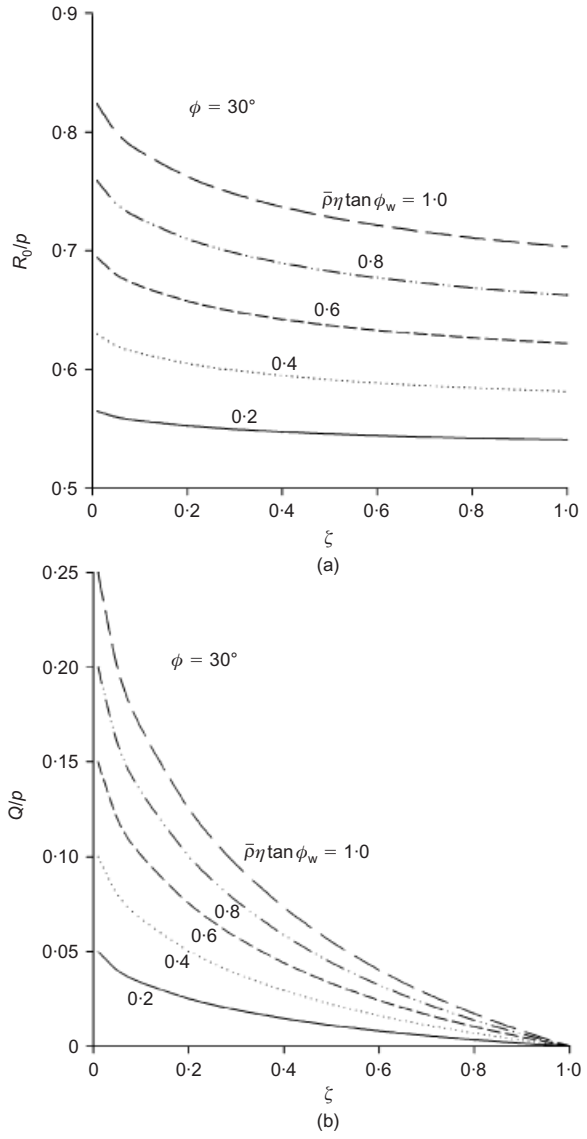

Fig. 10. Parameters (a) R_0 and (b) Q for the anisotropic yield condition

Table 1. R_0/p and Q/p for anisotropic fibre-reinforced sand

ϕ: degrees	$\bar{\rho}\eta \tan \phi_w$	ζ	R_0/p	Q/p
30	0·20	1·0	0·5406	0
		0·5	0·5456	0·0110
		0·2	0·5524	0·0251
	0·40	1·0	0·5812	0
		0·5	0·5912	0·0220
		0·2	0·6048	0·0502
	0·60	1·0	0·6218	0
		0·5	0·6368	0·0330
		0·2	0·6572	0·0753
35	0·20	1·0	0·6175	0
		0·5	0·6228	0·0116
		0·2	0·6298	0·0265
	0·40	1·0	0·6614	0
		0·5	0·6721	0·0233
		0·2	0·6861	0·0530
	0·60	1·0	0·7054	0
		0·5	0·7213	0·0349
		0·2	0·7424	0·0794
40	0·20	1·0	0·6899	0
		0·5	0·6956	0·0122
		0·2	0·7027	0·0277
	0·40	1·0	0·7372	0
		0·5	0·7484	0·0244
		0·2	0·7627	0·0555
	0·60	1·0	0·7844	0
		0·5	0·8012	0·0366
		0·2	0·8228	0·0834

The shape of the yield surface derived is dependent on the distribution of the fibre orientation, and for an ellipsoidal distribution the yield surface cross-section was found to be very close to a circle, although with some centre offset. One might expect that for other anisotropic distributions the cross-section of the yield surface might assume an elliptical shape, as the one first suggested in Fig. 8(b).

ANISOTROPY OF THE INTERNAL FRICTION ANGLE

Application of the kinematic approach of limit analysis requires calculations of the rate of internal and external work in collapse mechanisms. For a purely frictional material with linear yield condition the rate of internal work can be proven to be zero, as the stress and the associated strain-rate vectors are mutually orthogonal. However, the internal friction angle still needs to be evaluated for the fibre-reinforced soil, as it is needed to develop kinematically admissible failure mechanisms.

The angle of internal friction for an anisotropic material is dependent on the spatial direction, and the manner in which this angle is derived for a given inclination of the major principal stress is indicated in this section. For an isotropic, purely frictional material, the yield surface in space $\bar{\tau}_{xy}$, p, q is an axisymmetric cone, and the internal friction angle ϕ is described with the equation

$$\sin \phi = \frac{R}{p} \tag{30}$$

R is independent of ψ, as shown in Fig. 11(a): hence ϕ is not sensitive to the physical orientation. Angle ψ is the angle of inclination of the major principal stress to axis x, whereas ξ is the angle the major principal strain rate makes with axis x. Coaxiality of the two directions is characteristic of isotropic materials.

The yielding of an anisotropic composite is described here with a circular trace of the yield surface (cf. Fig. 9(b)), but

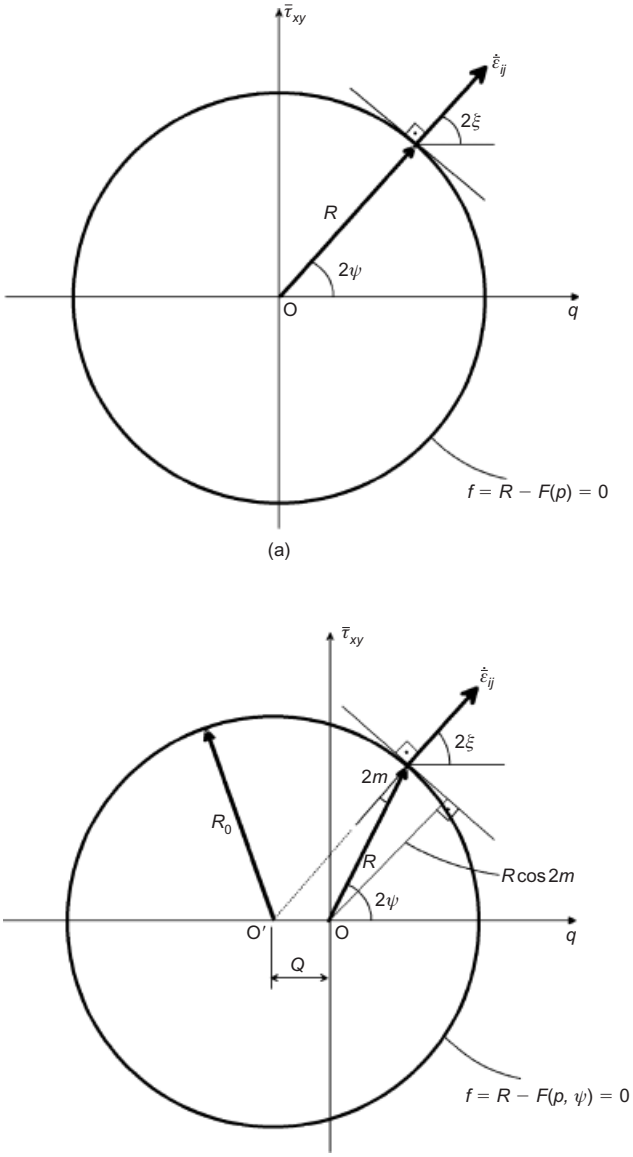

Fig. 11. Trace of the yield condition on plane p = constant: (a) isotropic soil; (b) anisotropic soil

this surface is now shifted with respect to the origin by distance Q along the q-axis (Fig. 11(b)). The internal friction angle ϕ_a for anisotropic material is now described by the expression

$$\sin \phi_a = \frac{R \cos 2m}{p} \tag{31}$$

where the 'noncoaxiality' angle m is shown in Fig. 11(b); it can also be found in Fig. 7 as the angle between $\bar{\sigma}_1$ and the major principal macroscopic strain rate direction. Both R and m are functions of ψ: thus angle ϕ_a depends on physical orientation, which is an attribute of anisotropy. Angle $2m$ in equation (31) can be determined easily from geometrical relations in Fig. 11(b) as

$$\sin 2m = \frac{Q}{R_0} \sin 2\psi \tag{32}$$

where Q/R_0 for a given sand–fibre mixture can be found from precalculated values in Table 1; radius R is

$$R = R_0 \frac{\sin 2\xi}{\sin 2\psi} \tag{33}$$

Consequently, angle ϕ_a can be calculated as a function of 2ψ

$$\sin\phi_a = \frac{R_0}{p}\left(\sqrt{1-\frac{Q^2}{R_0^2}\sin^2 2\psi} - \frac{Q}{R_0}\cos 2\psi\right)\sqrt{1-\frac{Q^2}{R_0^2}\sin^2 2\psi} \tag{34}$$

or, more concisely, as a function of angle 2ξ, after considering that $\psi = \xi + m$

$$\sin\phi_a = \frac{R_0}{p} - \frac{Q}{p}\cos 2\xi \tag{35}$$

It is noted that the relations in equations (34) and (35) were derived for the specific type of anisotropy illustrated in Fig. 9(b). Axis x with respect to which angles ψ and ξ are measured has a fixed orientation in the physical space. Here, it coincides with half-axis a of the ellipsoidal distribution of fibres (Fig. 7). It will be argued in the next section that the unique relation of the anisotropic internal friction angle ϕ_a to the principal stress (or strain rate) direction does not imply ϕ_a as a unique function of orientation in space.

An example of the variability of internal friction angle ϕ_a with a change in the principal stress direction (ψ) is shown in Fig. 12, for the fibre-reinforced sand with $\bar{\rho}\eta\tan\phi_w = 0{\cdot}4$ and sand internal friction angle $\phi = 30°$ (R_0/p and Q/p are given in Table 1). A uniform distribution of fibres in all directions ($\zeta = 1{\cdot}0$) leads, of course, to an internal friction angle that is independent of ψ (isotropy), more than 5° above the internal friction for the sand. Anisotropic distribution leads to varying ϕ_a. For a fibre distribution ratio of $\zeta = 0{\cdot}2$, the increase in the internal friction angle above that for the pure sand ranges from about 4° to 11°. The preferred bedding plane of the fibres is horizontal (coincides with axis x), and the largest increase occurs when $\psi = 90°$, that is, when the minor principal stress (or the maximum extension) coincides with the plane of the preferred fibre orientation. It is not surprising that, for some range of ψ, angle ϕ_a increases above that calculated for isotropic fibre distribution, and it is lower for the remaining range of ψ. The maximum increase above the isotropic value $\bar{\phi}$ (at $\psi = 90°$), however, is larger than the relative decrease (at $\psi = 0$). This is because the number of fibres contributing to the strength (subjected to tension) under different deformation regimes is affected by the distribution of fibre orientation. For the same reason, the radius of the yield condition R in Fig. 9(a) was dependent on the orientation of fibres.

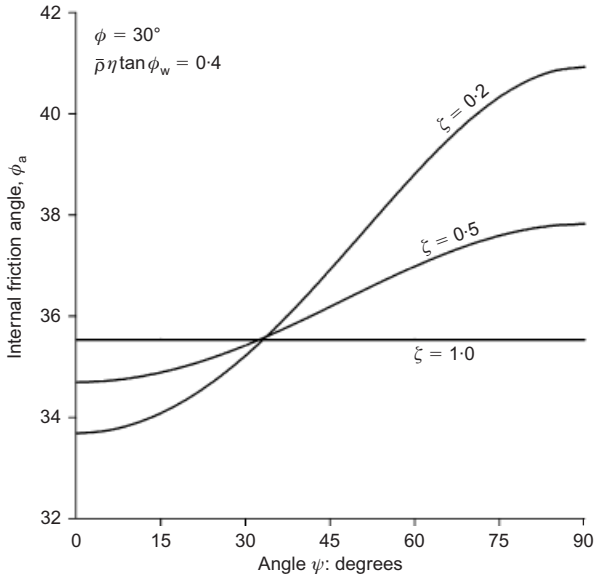

Fig. 12. Internal friction angle as a function of the major principal stress inclination to the preferred fibre orientation plane

For fibre-reinforced sand with isotropic distribution of fibre orientation, a closed-form solution to the internal friction angle $\bar{\phi}$ can be found as

$$\bar{\phi} = \arcsin\left(\sin\phi + \frac{1}{3}N\bar{\rho}\eta\tan\phi_w\right) \tag{36}$$

where N is given in equation (29). This isotropic internal friction angle is slightly different from the one derived for axisymmetric deformation (Michalowski & Čermák, 2003).

ADMISSIBLE FAILURE MECHANISMS

Admissible mechanisms of failure can exhibit velocity discontinuities, with adjacent regions moving as rigid blocks or as regions undergoing continual deformation. For the limit analysis theorems to be applicable, the deformation must conform to the associative flow rule. We shall concentrate here only on mechanisms that consist of rigid blocks separated by velocity discontinuities.

The yield condition in equation (19) along with the differential equations of equilibrium leads to a set of hyperbolic-type differential equations for the description of the plastic stress state. The equations describing the associated kinematics (velocities) are also of the hyperbolic type, and the characteristics of the two sets of equations coincide (Booker & Davis, 1972); they can be written as

$$\frac{dy}{dx} = \tan(\psi - m \pm \nu) = \tan(\xi \pm \nu), \qquad \alpha,\ \beta \tag{37}$$

with the upper sign referring to characteristics of the α-family, and lower to family β. For the linear yield condition, angle ν can be shown to be equal to

$$\nu = \frac{\pi}{4} - \frac{\phi_a}{2} \tag{38}$$

Hence both the stress and velocity characteristics are inclined to the major principal strain rate direction at angles $\pm\nu$.

As in the isotropic materials, velocity discontinuities in anisotropic media must be velocity characteristics. Since the normality flow rule is used in limit analysis, the dilatancy angle that the velocity 'jump' vector makes with the velocity discontinuity is equal to internal friction angle ϕ_a. This angle must be known in order to construct kinematically admissible mechanisms. Angle ϕ_a is a function of the major principal stress direction (see equation (34) and Fig. 12); however, in the kinematic approach principal stress directions are not determined directly. Rather, principal stress directions can be incurred from the spatial orientation of the kinematic discontinuity, since such discontinuities must be velocity characteristics, and those have a well-defined inclination with respect to the major principal stress direction (see equation (37)). Because the kinematic discontinuity can belong to either an α- or a β-family, the resulting ϕ_a along a velocity discontinuity is not unique. While it is possible, for a given boundary value problem, to determine whether a discontinuity coincides with a characteristic of α- or β-family, and thus to determine a unique value of ϕ_a along that discontinuity, the internal friction angle cannot be determined *a priori* as a unique function of orientation in space.

Alternatively, the angle of internal friction ϕ_a can be

represented as a function of the angle of major principal strain rate direction ξ, as in equation (35). Angle ξ, however, can be determined only when the relative velocities of regions on both sides of the discontinuity are known. Thus angle ϕ_a cannot be defined as a unique function of orientation, before the kinematics of the problem (mechanism) are defined.

In constructing admissible velocity fields (failure mechanisms), one first assumes hypothetical inclinations of all velocity discontinuities. Then, based on this geometry, the hodograph is constructed. However, the dilatancy angle on each discontinuity must be determined before the hodograph can be constructed. The procedure of evaluating ϕ_a on all discontinuities is iterative. This is because the angle of inclination of a discontinuity to axis x must be equal to $\xi \pm (\pi/4 - \phi_a/2)$ (Fig. 13), where ϕ_a and ξ are not independent, but are related through equation (35).

EXAMPLES

Two examples are selected to illustrate the use of the kinematic approach of limit analysis in anisotropic media: active load on a vertical rough retaining wall, and the bearing capacity of a strip footing. The first example involves only one velocity discontinuity in the mechanism (Fig. 14). Since internal work during plastic deformation of the composite considered is equal to zero, the only two terms in the work balance equation are those due to the weight of the soil and force P_a resisting the failure

$$0 = \frac{\gamma H^2}{2}\cot\theta V \sin(\theta - \phi_a) - P_a V_{wall}\cos\delta \tag{39}$$

where δ is the angle of friction at the wall/soil interface. Now, using the geometric relations in the hodograph, Fig. 14(b), one obtains the expression for the load on the wall

$$P_a = \frac{\gamma H^2}{2}\cot\theta \frac{\sin(\theta - \phi_a)}{\cos(\theta - \phi_a - \delta)} = \frac{\gamma H^2}{2} K_a \tag{40}$$

Because force P_a is the wall reaction, this approach yields the lower bound to P_a, and the maximum is sought from equation (40) with θ being variable. The discontinuity AB in Fig. 14(a) coincides with a characteristic of family β (cf. Fig. 13): therefore

$$\theta = \xi - \frac{\pi}{4} + \frac{\phi_a}{2} \tag{41}$$

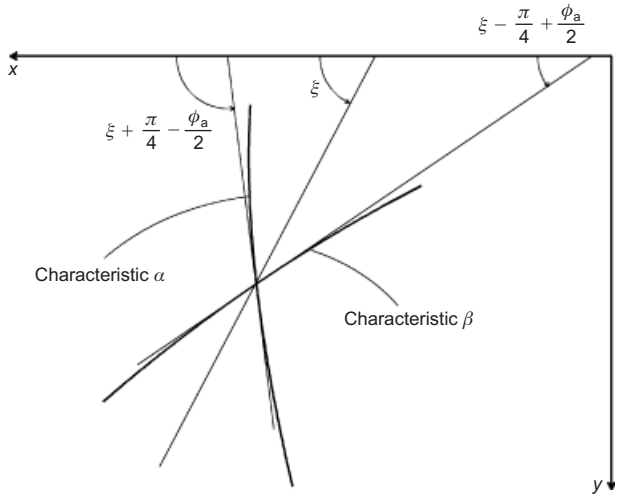

Fig. 13. Velocity characteristics

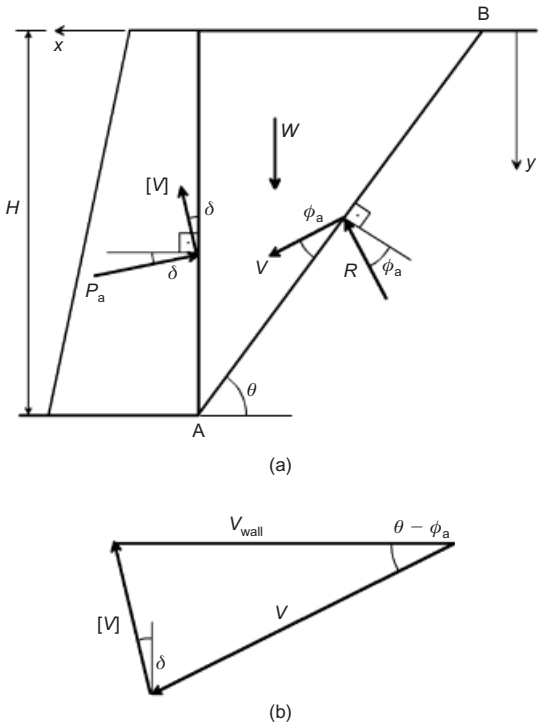

Fig. 14. Retaining wall example: (a) geometry; (b) hodograph

but the internal friction angle ϕ_a varies with inclination θ. Eliminating ξ from equation (35) by using (41), one obtains

$$\sin\phi_a - \frac{Q}{p}\sin(2\theta - \phi_a) - \frac{R_0}{p} = 0 \tag{42}$$

Table 2. Load coefficient K_a for rough vertical wall

ϕ: degrees	δ: degrees	$\bar{\rho}\eta\tan\phi_w$	ζ	K_a
30	15	0	–	0·301
		0·2	1·0	0·271
			0·5	0·260
			0·2	0·245
		0·4	1·0	0·242
			0·5	0·221
			0·2	0·193
		0·6	1·0	0·215
			0·5	0·184
			0·2	0·145
35	15	0	–	0·248
		0·2	1·0	0·218
			0·5	0·207
			0·2	0·192
		0·4	1·0	0·189
			0·5	0·168
			0·2	0·141
		0·6	1·0	0·162
			0·5	0·131
			0·2	0·094
40	15	0	–	0·201
		0·2	1·0	0·171
			0·5	0·160
			0·2	0·146
		0·4	1·0	0·142
			0·5	0·121
			0·2	0·096
		0·6	1·0	0·115
			0·5	0·085
			0·2	0·048

Now, for a given inclination θ of the velocity discontinuity in Fig. 14(a), the internal friction angle ϕ_a was found iteratively from equation (42), and the maximum coefficient K_a in equation (40) was evaluated (with θ being variable); R_0/p and Q/p were taken from Table 1. The results are presented in Table 2 for different fibre properties $\bar{\rho}\eta \tan \phi_w$, and distribution ratio ζ. The addition of fibres to the backfill reduces the load on the wall, measured in the reduction in the coefficient K_a. Not surprisingly, the load decreases with increase of the concentration of fibres in the backfill, but it is also affected by the distribution of fibre orientation. The horizontal preferred bedding plane contributes significantly to the reduction in the wall load.

The second example is the bearing capacity of a surface footing. The multi-block mechanism in Fig. 15(a) is now considered. The bearing capacity (average stress) is considered in the form

$$\bar{p} = \frac{1}{2}\gamma B N_\gamma \tag{43}$$

where N_γ is often referred to as the bearing capacity factor. This mechanism was used earlier to calculate the bearing capacity of isotropic soils (Michalowski, 1997b), and a closed-form approximation of the numerical solution was found as

$$N_\gamma = e^{0{\cdot}66+5{\cdot}11 \tan \phi} \tan \phi \tag{44}$$

For a general case of anisotropy the mechanism is not symmetric; however, the pattern of anisotropy considered here is symmetric, with the horizontal being the preferred fibres bedding plane. Therefore only one half of the mechanism is considered.

The procedure for bearing capacity calculations is the same as that in Michalowski (1997b), but the angle of internal friction now varies, depending on the angle of inclination of the discontinuity surfaces. Discontinuity *ABC ... F* coincides with the characteristic of the α-family, whereas the discontinuities originating from point O all coincide with the characteristics of family β.

The discontinuity segments are described by their inclination angles θ_α and θ_β, as shown in Fig. 14(b). These inclinations are known in a given failure mechanism, and, along with equation (35), they form a set of equations from which the internal friction angle ϕ_a on every discontinuity was evaluated. In the next step, the velocities were calculated from the geometrical relations in the hodograph (Fig. 14(c)), and the limit load on the footing was calculated from the work balance in the mechanism. The upper bound of the limit load so obtained was minimised with respect to all independent angles describing the geometry of the mechanism, and coefficient N_γ (equation (43)) was inferred from the calculated limit load. With every change of the inclination of the discontinuities in the mechanism during the optimisation process, new values of internal friction angle ϕ_a along all discontinuities were calculated. A symmetric half of the mechanism with 50 blocks was used in calculations. The results are shown in Table 3 (three digits after the decimal point are given for comparative reasons only, and it is not to suggest that the bearing capacity so calculated is that precise).

As the internal friction of sand is increased with the addition of fibres, the bearing capacity factor N_γ also increases. The anisotropic distribution of fibre orientation contributes further to this increase: that is, the distribution

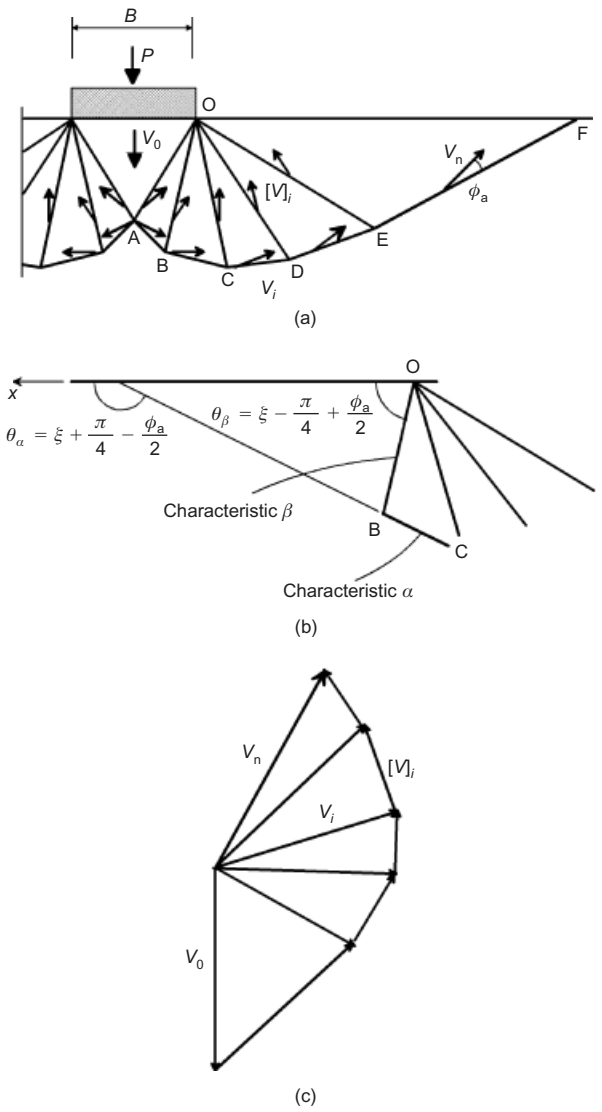

Fig. 15. Strip footing: (a) failure mechanism; (b) inclination of discontinuities related to principal strain rate direction; (c) hodograph

Table 3. Bearing capacity factor N_γ for anisotropic fibre-reinforced sand (rough footing)

ϕ: degrees	$\bar{\rho}\eta \tan \phi_w$	ζ	N_γ
30	0	–	21·394
	0·2	1·0	33·239
		0·5	35·775
		0·2	39·598
	0·4	1·0	53·301
		0·5	62·636
		0·2	79·380
35	0	–	48·681
	0·2	1·0	84·305
		0·5	92·280
		0·2	104·612
	0·4	1·0	155·559
		0·5	191·827
		0·2	263·931
40	0	–	118·826
	0·2	1·0	241·893
		0·5	272·732
		0·2	321·365
	0·4	1·0	561·436
		0·5	755·590
		0·2	1207·296

of fibres with the horizontal preferred plane benefits the bearing capacity more than the isotropic distribution.

FINAL REMARKS

A yield condition for fibre-reinforced sand with ellipsoidal distribution of fibres was developed. The yield condition is anisotropic, and the maximum shear stress can be represented as a function of the inclination of the principal stress direction and the in-plane mean stress. Numerical simulations revealed that the trace of the yield condition on plane q, $\bar{\tau}_{xy}$ ($q = (\bar{\sigma}_x - \bar{\sigma}_y)/2$) can be represented as a circle with its centre moved along q, giving rise to anisotropic shear strength.

The yield condition developed was used in the kinematic approach of limit analysis. As the material is anisotropic, the internal friction angle ϕ_a is not unique. This angle can be represented as a function of the major principal stress (or strain rate) direction, but it cannot be determined *a priori* as a unique function of orientation in space. However, for a given boundary value problem the principal strain rate directions can be incurred from the kinematics of the mechanism, and a unique value of ϕ_a can be found iteratively along all velocity discontinuities.

Two examples were presented to illustrate the use of the kinematic approach for anisotropic frictional materials. Solutions to a rough retaining wall loading and the bearing capacity of a strip footing indicated that the addition of fibres reduces the load on the retaining walls, and increases the bearing capacity. In both cases, the contribution of the fibres was enhanced by anisotropic distribution of their orientation.

ACKNOWLEDGEMENTS

The work presented in this paper was carried out while the author was supported by the National Science Foundation, grant No. CMMI-0724022, and the Army Research Office, grant No. DAAD19–03–1–0063. This support is greatly appreciated.

APPENDIX

The rate of internal work for a single fibre in pure slip mode is expressed in equation (4), and the integrated rate of work dissipation in all fibres is needed in equation (17). For integration purposes, volume V in equation (17) is taken as a sphere (integration space), and all fibres are moved (fictitiously) in a parallel manner so that the mid-point of each fibre is placed at the centre of the sphere. Such an operation is admissible because the deformation is assumed to be uniform, and the work dissipation associated with a single fibre is dependent only on its orientation and not on its location in the specimen. In this integration space, it is possible to separate the fibres under compression from those in tension. In integration of the work rate over all fibres, those under compression can be excluded simply by adjusting the limits of integration.

The integration space is illustrated in Fig. 16; only a quarter-sphere volume needs to be considered. The average fibre content in volume V is expressed in equation (8), and the number of fibres in volume V can be found as

$$n = \frac{\bar{\rho}}{\pi r^2 l} V = \frac{4\bar{\rho}\eta^2}{\pi l^3} V = \frac{4\eta^2}{\pi l^3} \int_V \rho(\theta) \mathrm{d}V \tag{45}$$

Utilising equation (4), the rate of internal work per unit volume in the quarter spherical specimen V becomes

$$D_f = \frac{1}{\frac{1}{3}\pi R_0^3} \int_V \rho(\theta) \eta \bar{\sigma}_n \tan\phi_w \langle \dot{\varepsilon}_\theta \rangle \mathrm{d}V \tag{46}$$

The strain rate $\langle \dot{\varepsilon}_\theta \rangle$ is a function of inclination angle θ, and the procedure for integration is described below, including an explanation of how the fibres in compression are excluded from the integral.

The principal directions of the strain rate coincide with axes x' and y' in the integration space (Fig. 16), and the velocities are ($\dot{\bar{\varepsilon}}_z = 0$)

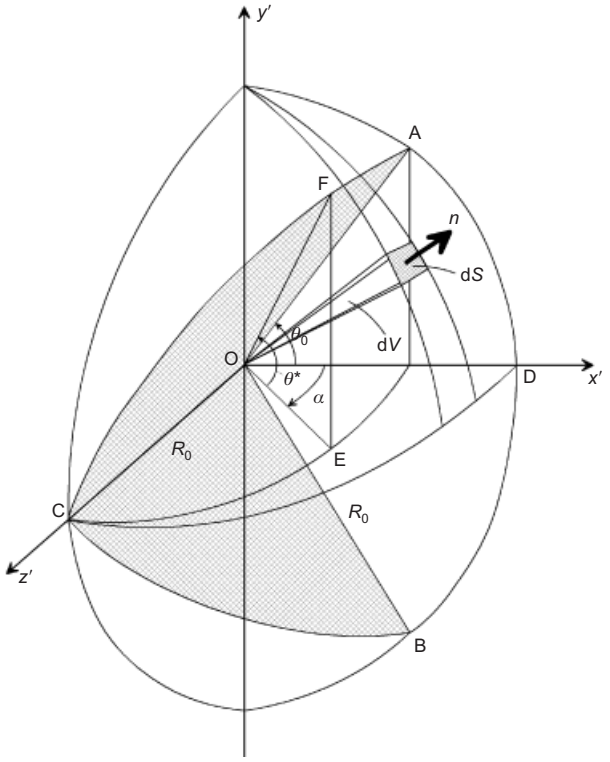

Fig. 16. Integration space

$$\mathbf{v} = -\dot{\bar{\varepsilon}}_3 x' \mathbf{i} - \dot{\bar{\varepsilon}}_1 y' \mathbf{j} \tag{47}$$

where $\mathbf{i}$ and $\mathbf{j}$ are the unit vectors in the directions x' and y' respectively. The unit vector $\mathbf{n}$ perpendicular to the surface of the spherical integration space is

$$\mathbf{n} = \frac{x'}{R_0}\mathbf{i} + \frac{y'}{R_0}\mathbf{j} + \frac{z'}{R_0}\mathbf{k} \tag{48}$$

and the strain rate in the direction inclined at angle θ to the horizontal is ($\dot{\bar{\varepsilon}}_z = \dot{\bar{\varepsilon}}_2 = 0$)

$$\dot{\bar{\varepsilon}}_\theta = -\frac{\mathbf{v}\cdot\mathbf{n}}{R_0} = \frac{\dot{\bar{\varepsilon}}_3 x'^2 + \dot{\bar{\varepsilon}}_1 y'^2}{R_0^2} = \dot{\bar{\varepsilon}}_1 \sin^2\theta + \dot{\bar{\varepsilon}}_3 \cos^2\alpha \cos^2\theta \tag{49}$$

Because all fibres were fictitiously moved with their mid-points to the origin, and the plane strain condition is considered, the fibres in compression are separated from those in tension by two shaded planes shown in Fig. 16 (OCB and OCA). Angle θ_0 of inclination of these planes to plane $x'Oz'$ is found from the zero strain condition

$$\dot{\bar{\varepsilon}}_{\theta_0} = \dot{\bar{\varepsilon}}_1 \sin^2\theta_0 + \dot{\bar{\varepsilon}}_3 \cos^2\theta_0 = 0 \tag{50}$$

leading to (after using equation (18))

$$\theta_0 = \pm\left(\frac{\pi}{4} + \frac{\phi}{2}\right) \tag{51}$$

Now make an approximation that the average stress on a single fibre $\bar{\sigma}_n$ is independent of the fibre orientation (i.e. constant), and it is approximately equal to in-plane mean stress p (equation (21)). Replacing $\langle \dot{\bar{\varepsilon}}_\theta \rangle$ in equation (46) with the strain rate in equation (49), and using equation (18) to eliminate $\dot{\bar{\varepsilon}}_3$, the volume integral in equation (46) can be transformed into ($\mathrm{d}V = R_0 \mathrm{d}S/3 = R_0^3 \cos\theta \mathrm{d}\alpha \mathrm{d}\theta/3$)

$$D_f = \frac{1}{\pi} p\eta \tan\phi_w \dot{\bar{\varepsilon}}_1 \int_0^{\frac{\pi}{2}} \int_{-\theta^*}^{\theta^*} \rho(\theta) \left| \sin^2\theta - K_p \cos^2\alpha \cos^2\theta \right| \cos\theta \mathrm{d}\theta \mathrm{d}\alpha \tag{52}$$

The absolute value of the trigonometric expression in equation (52) is taken because of the definition of $\langle \dot{\bar{\varepsilon}}_\theta \rangle$ in equation (3). The

integration is performed over the volume between the two shaded planes in Fig. 16 (fibre tension region), and the limits of θ are $\mp\theta^*$, where $\theta^* = \arctan(\cos\alpha \tan\theta_0)$. Once the internal work is calculated from equation (52), the limit shear stress R can be evaluated from equation (27), and the yield surface determined (cf. Fig. 9).

Because the bedding plane, in general, is different from axis x' in Fig. 7 (it does not coincide with plane $x'Oz'$ in the integration space in Fig. 16), the orientation distribution in the dissipation function in equation (52) must be altered to read

$$\rho(\theta) \rightarrow \rho(\theta - \omega^*) = \frac{ab}{\sqrt{a^2 \sin^2(\theta - \omega^*) + b^2 \cos(\theta - \omega^*)}} \quad (53)$$

where $\omega^* = \arctan(\cos\alpha \tan\omega)$ (see Fig. 7 for ω).

NOTATION

- a, b half-axes of ellipsoidal fibre orientation distribution function
- D_f work rate dissipation function
- d rate of work dissipation per single fibre
- I_1 integral used in fibre orientation distribution function
- K_p function of internal friction angle ϕ
- l fibre length
- m non-coaxiality angle
- p in-plane mean stress $(\bar{\sigma}_x + \bar{\sigma}_y)/2$
- Q shift of the yield function
- q stress function $(\bar{\sigma}_x - \bar{\sigma}_y)/2$
- R shear strength defined in equation (20)
- R_0 radius of the circular yield condition (also, radius of the integration space)
- r fibre radius
- s length of fibre slip section
- V element volume
- V_r volume of fibres
- α spherical co-ordinate
- γ unit weight of soil
- $\dot{\bar{\varepsilon}}_1$, $\dot{\bar{\varepsilon}}_3$ major and minor principal strain rates in composite (averaged over composite constituents)
- $\dot{\bar{\varepsilon}}_x$, $\dot{\bar{\varepsilon}}_y$ normal strain rate components (averaged over composite constituents)
- $\langle\dot{\varepsilon}_\theta\rangle$ matrix strain rate in the direction of fibre inclined at angle θ (positive if extension, zero otherwise)
- ζ distribution ratio defined in equation (12)
- η fibre aspect ratio
- θ spherical co-ordinate
- ξ inclination angle of the major principal strain rate to x-axis
- ρ fibre orientation distribution function
- $\bar{\rho}$ mean volumetric fibre concentration
- $\bar{\sigma}_1$, $\bar{\sigma}_3$ major and minor principal stresses in composite (averaged over composite constituents)
- $\bar{\sigma}_x$, $\bar{\sigma}_y$ composite normal stresses (averaged over composite constituents)
- $\bar{\tau}_{xy}$ composite shear stress
- ϕ internal friction angle of sand
- ϕ_a internal friction angle for anisotropic material
- ϕ_w fibre-matrix interface friction angle
- ψ inclination angle of the major principal stress to x-axis
- ω inclinaton of preferred bedding plane to x'-axis

REFERENCES

Booker, J. R. & Davis, E. H. (1972). A general treatment of plastic anisotropy under conditions of plane strain. *J. Mech. Phys. Solids* **20**, No. 4, 239–250.

Consoli, N. C., Casagrande, M. D. T. & Coop, M. R. (2005). Effect of fiber reinforcement on the isotropic compression behavior of sand. *J. Geotech. Geoenviron. Engng* **131**, No. 11, 1434–1436.

Diambra, A., Russell, A. R., Ibraim, E. & Muir Wood, D. (2007). Determination of fibre orientation distribution in reinforced sands. *Géotechnique* **57**, No. 7, 623–628.

Gray, D. H. & Ohashi, H. (1983). Mechanics of fiber reinforcement in sand. *J. Geotech. Engng* **109**, No. 3, 335–353.

Hausmann, M. R. (1976). Strength of reinforced soil. *Proc. 8th Australian Road Research Conf.*, Perth, **8**, Sect. 13, 1–8 (cited after Maher, 1988).

Leflaive, E. & Liausu, Ph. (1986). The reinforcement of soils by continuous threads. *Proc. 3rd Int. Conf. on Geotextiles, Vienna* **4**, 1159–1162.

Maher, M. H. (1988). *Static and dynamic response of sands reinforced with discrete, randomly distributed fibers*. Doctoral dissertation, University of Michigan, Ann Arbor.

Maher, M. H. & Gray, D. H. (1990). Static response of sands reinforced with randomly distributed fibers. *J. Geotech. Engng* **116**, No. 11, 1661–1677.

Michalowski, R. L. (1997a). Limit stress for granular composites reinforced with continuous filaments. *ASCE J. Engng Mech.* **123**, No. 8, 852–859.

Michalowski, R. L. (1997b). An estimate of the influence of soil weight on bearing capacity using limit analysis. *Soils Found.* **37**, No. 4, 57–64.

Michalowski, R. L. & Čermák, J. (2002). Strength anisotropy of fiber-reinforced sand. *Comput. Geotech.* **29**, No. 4, 279–299.

Michalowski, R. L. & Čermák, J. (2003). Triaxial compression of sand reinforced with fibers. *J. Geotech. Geoenviron. Engng* **129**, No. 2, 125–136.

Michalowski, R. L. & Zhao, A. (1996). Failure of fiber-reinforced granular soils. *J. Geotech. Geoenviron. Engng ASCE* **122**, No. 3, 226–234.

di Prisco, C. & Nova, R. (1993). A constitutive model for soil reinforced by continuous threads. *Geotextiles and Geomembranes* **12**, No. 2, 161–178.

Waldron, L. J. (1977). The shear resistance of root-permeated homogeneous and stratified soil. *J. Soil Sci. Soc. Am.* **41**, No. 5, 843–849.

Zornberg, J. G. (2002). Discrete framework for limit equilibrium analysis of fibre-reinforced soil. *Géotechnique* **52**, No. 8, 593–604.